


Review

MXenes: promising 2D memristor materials for neuromorphic computing components

Monika Patel,¹ Neelgund Ramesh Hemanth,² Jeny Gosai,¹ Ranjit Mohili,¹ Ankur Solanki,^{3,*} Mohendra Roy,^{4,*} Baizeng Fang ,^{5,*} and Nitin K. Chaudhari^{1,*}

Brain-inspired parallel computing ‘neuromorphic computing’ is one of the most promising technologies for efficiently handling large amounts of information data, which operates based on a hardware-neural network platform consisting of numerous artificial synapses and neurons. Memristors, as artificial synapses based on various 2D materials for neuromorphic and data storage technologies with low power consumption, high scalability, and high speed, have been developed to address the von Neumann bottleneck and limitations of Moore’s law. The 2D MXenes have strong potential application in memristors due to their ultrahigh conductivity, fast charge response, high stacking density, and high hydrophilicity. Here, we discuss how MXenes are emerging as a potential material towards artificial synapses. Recent progress in research on artificial synapses, fabricated particularly using MXenes and their composite materials, is comprehensively discussed with respect to mechanism, synaptic characteristics, power efficiency, and scalability. Finally, we present an outlook of the future development of MXenes for artificial intelligence and challenges in integrating memristors with MXenes are briefly discussed.

MXenes: an emerging material for neuromorphic computing

Recent advances in artificial intelligence (AI) and machine learning (ML) have significantly influenced the development of state-of-the-art electronic devices for advanced applications. Sustaining such a high growth rate has resulted in an increased demand for ‘universal memory’ devices with outstanding capabilities such as high data transfer speed, storage capacity, nonvolatility, and low operation voltage. Particularly, deep neural networks show tremendous possibility for large-scale data storage, processing, and prediction, which are very complex with thousands of parameters that must be optimized during the learning process of AI [1,2]. These learning processes are computationally and memory-wise very intensive, which significantly increases the complexity and could easily exhaust traditional computation machines [3]. However, an efficient and more powerful computing structure, the human biological brain, can handle much higher degrees of complexity both in terms of computation as well as memory in a very power-efficient manner [4]. The human brain is capable of processing complex information in a fraction of a second as it consists of hundreds of billions of neurons (10^{11}) and several hundred trillions of synaptic connections (10^{15} synapses) that play an important role in memory, learning cognition, and decision-making [5]. The brain can also store 10^9 bits of information, which is 50 000 times higher than the text contained in the US Library of Congress [5,6]. Generally, the human brain consumes very low energy to complete the abovementioned tasks; on average it consumes only 20% of total body energy (20–30 W) [7–9]. However, traditional computers, which are inferior to the human brain, consume much more power (around 100 W) and the main disadvantage of traditional computer architecture is the **von Neumann bottleneck** (see Glossary) (Figure 1A) [10].

Highlights

Inspired by the human brain, neuromorphic computing uses artificial synapses and the network of neurons to realize the ability for parallel computing, progressive inference, and learning. This evolving technology can transcend the current limitations of von Neumann computing architectures.

Memristors are nonlinear resistance switching devices with memory functions that can mimic brain-like synapses. The in-memory computation feasibility of memristors is the major advantage. They have potential application in AI and neural computing due to their rapid switching speed, storage density, low power consumption, superior data processing capabilities, and can be simulated on a biological scale.

Owing to their excellent conductivity, hydrophilic surface, fast charge response, high stacking density, and durability, 2D MXenes are emerging as potential materials for memristors.

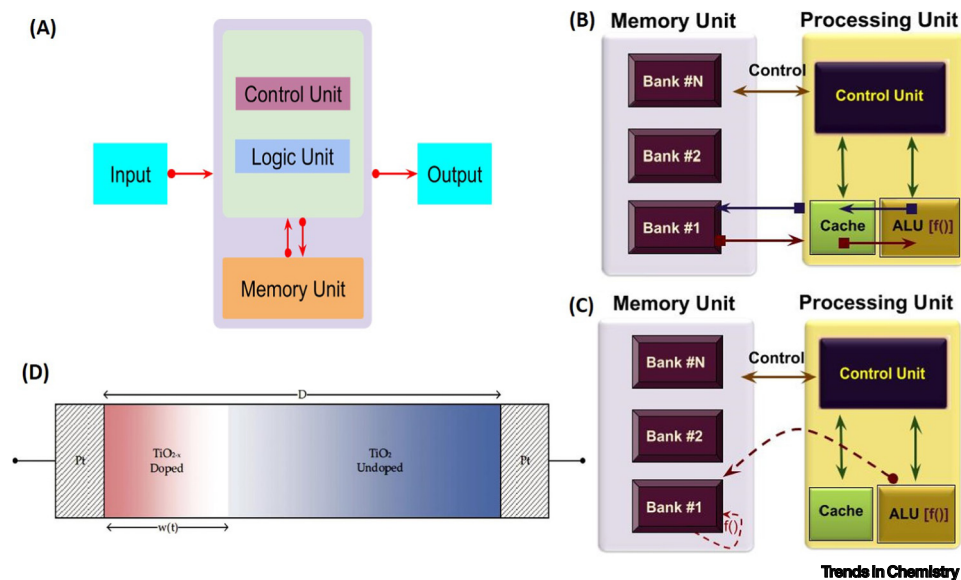
¹Department of Chemistry, School of Technology, Pandit Deendayal Energy University, Gandhinagar 382426, Gujarat, India

²Department of Metallurgical and Materials Engineering, National Institute of Technology Karnataka (NITK), Surathkal 575025, Karnataka, India

³Department of Physics, School of Technology, Pandit Deendayal Energy University, Gandhinagar 382426, Gujarat, India

⁴Department of Information and Communication Technology, School of Technology, Pandit Deendayal Energy University, Gandhinagar 382426, Gujarat, India

⁵Department of Chemical and Biological Engineering, University of British Columbia, 2360 East Mall, Vancouver, BC, V6T 1Z3, Canada



*Correspondence:
 ankur.solanki@sot.pdpu.ac.in (A. Solanki),
 mohendra.roy@sot.pdpu.ac.in (M. Roy),
 bfang@chbe.ubc.ca (B. Fang), and
 nitin.chaudhari@sot.pdpu.ac.in
 (N.K. Chaudhari).

Figure 1. Von Neumann architecture, in-memory computation, and structure of a memristor. (A) Von Neumann architecture. Comparison between traditional computation and in memory computation. (B) Traditional von Neumann architecture. (C) In-memory computation. (D) Structure of memristor reported by Hewlett Packard (HP) laboratory. Reproduced, with permission, from [48].

Consequently, researchers are trying to mimic the architecture of the biological brain by developing computing devices and systems to realize an electronic brain, which leads to the incarnation of neuromorphic computing. In 1990, Carver Mead had coined the term 'neuromorphic engineering' for his work on brain-inspired analog computing hardware for pattern recognition [11]. Synapses are a means to pass information to other cells, which are also a unit of computation [4]. The electrical synapse in the biological brain is very effective due to its bidirectional nature [12]. The basic synaptic characteristics, such as nonlinear transmission characteristics, **spike-timing-dependent plasticity (STDP)**, **spike-rate-dependent plasticity (SRDP)**, **short-term plasticity (STP)**, and **long-term plasticity (LTP)**, are the major functions; these characteristics can be mimicked using memristor-based artificial synapses [13,14].

Memristors are nonvolatile two-terminal devices (whose fundamental property is programmable resistance) that can be used as memory. Additionally, the **resistive switching (RS)** property of the memristor can be utilized like a traditional transistor as a fundamental computation unit. The characteristics of memristors, as a function of the current flowing through, renders them suitable for mimicking the behavior of brain synapses, especially the plasticity of the brain neuron [15]. As a result, memristors can be used in memory computation [16] by easing read and write operations as logical operations and the comparison between traditional **von Neumann architecture** and in-memory computation (Figure 1B,C) [17]. The resistance of memristors is voltage dependent, which can be reversibly changed and completed by sandwiching thin films of semiconducting materials in between two metal electrodes [18]. The RS properties of these devices can be controlled by growth and breakage of the conductive filaments (CFs) between two metal electrodes [19]. However, metal oxide-based device structures suffer from spatial and temporal device variations [20]. Hybrid organic-inorganic perovskites [21–23] are found to be an efficient and low-temperature processing alternative to the oxides but scaling and reproducibility are challenging due to their instability over a long period. Researchers are now

experimenting with 2D materials such as molybdenum disulfide, reduced graphene oxide, black phosphorus, and boron nitride [24]. Transition metal carbides and nitrides (namely MXenes) also have gained significant interest due to their excellent electrical conductivity, wide band gap, good thermal conductivity, and easy processability; these can be excellent materials for the development of robust memristors and electronic synaptic devices for next-generation applications [2,25–28].

Since the first discovery of $Ti_3C_2T_x$ in 2011 [29], various MXenes have been extensively studied based on combinations of different transition metals and their alloys with C and N [30]. MXenes have shown exciting potential for a wide range of applications, owing to their well-designed architecture, high specific surface area and large interlayer distancing, excellent thermal and electrical conductivity, adjustable hydrophobicity, and ease of functionalization [31–45]. However, neuromorphic computing and AI are newly promising and emerging fields for MXenes, with both immense potential and challenges [42]. Various nanostructured materials have been examined due to ease of processing, low operating voltage, low cost, and high compatibility with flexible applications. However, the inability to perform long-term operation under harsh ambient conditions encourages MXenes as an attractive alternative for neuromorphic computing [33,34,43–45]. This review discusses the recent development of memristors and their applications for data storage and neuromorphic computing based on MXenes, which are playing an increasingly important role in diverse fields, including artificial synapses and data storage. We believe that the present review will assist in developing memristors for next-generation information technology in more systematic ways.

Fundamentals of memristors, device configuration, and switching mechanism

Memristors are a nonlinear electrical component with the capability of programmable device resistance [46]. The first memristor was physically fabricated by the HP research laboratory in 2008, composed of a Pt/TiO₂/Pt sandwich-like structure (Figure 1D) [47]. Memristor devices have a sandwich-type structure consisting of an electrode/active material/electrode configuration, which is energy efficient and immune to radiation. The relationship between current (i), voltage (V), charge (q), and flux (ϕ) for the memristor is given by the following equations [48]:

$$V(t) = M[q(t)]i(t) \quad [1]$$

where

$$M[q(t)] = \frac{d\phi(q)}{dq} \quad [2]$$

and

$$i(t) = W[\phi(t)]V(t) \quad [3]$$

Here, $W[\phi(t)] = \frac{dq(\phi)}{d\phi}$, $M[q(t)]$ is resistance, and $W[\phi(t)]$ is conductance. The nonvolatile memory effect can be described by

$$V(t) = M\left[\int_{-\infty}^t i(t)dt\right]i(t) \quad [4]$$

Equation [4] indicates that resistance is a function of current at a given time and the general mechanism of RS in memristor devices is shown by measured I-V characteristics (Figure 2A).

Glossary

High resistance state (HRS): a state of material with high resistance under the influence of external force.

Long-term plasticity (LTP): the weight change in synapse for long duration after applied voltage spikes.

Low resistance state (LRS): a state of material with low resistance under the influence of an external field.

MAX phases: layered, hexagonal carbide and nitride materials that bridge the gap between properties typical of metals and ceramics.

Resistive switching (RS): a physical phenomenon where a dielectric changes its resistance with respect to the applied electric field or current.

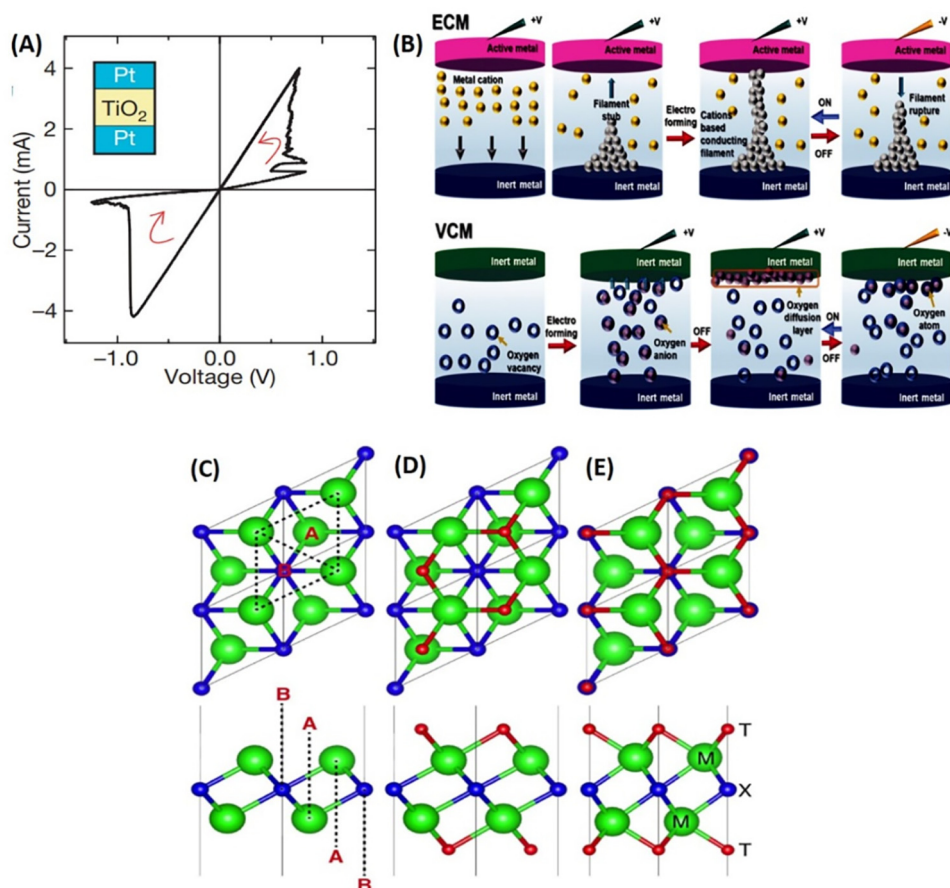
Short-term plasticity (STP): weight change in synapse for short duration after voltage spikes.

Spike-rate-dependent plasticity (SRDP): synapse weight change with respect to frequency of applied voltage spikes.

Spike-timing-dependent plasticity (STDP): synapse weight change with respect to time duration of applied voltage spikes.

Von Neumann architecture: traditional computer architecture, consists of separate memory and processor units.

Von Neumann bottleneck: limitation on throughput caused by the separate memory and processor units.



Trends in Chemistry

Figure 2. Experimental I–V plot, operating mechanism, and top and side views of models for functionalized MXenes. (A) Experimental I–V plot of a Pt/TiO_{2-x}/Pt device. Reproduced, with permission, from [47]. (B) Operating mechanism of resistive switching behavior; electroforming process, filament formation, and rupture in the switching layer (from left to right). Reproduced, with permission, from [104]. (C–E) Top and side views of F pristine MXene M₂X. Top and side views of (D) model 2 and (E) model 4 for functionalized MXene (see main text). (D) and (E) indicate different types of hollow sites in (C). M, X, and T denote transition metal (green), C/N (blue), and attached chemical groups such as F, O, and OH (red), respectively. Reproduced, with permission, from [105]. Abbreviations: ECM, electrochemical metallization; VCM, valence change mechanism.

The fundamental operational mechanism of memristors is analogous to conventional flash memory [49,50]. A positive voltage pulse above a threshold voltage is applied to change the device resistance from a **high resistance state (HRS)** (unprogrammed in flash memory) to a **low resistance state (LRS)** (programmed in flash memory), which is known as a SET process, with the required voltage for the write process as the SET voltage. The amount of voltage pulse determines the resistance of the memristor. The LRS or HRS states are established by applying voltage pulses of a certain polarity (i.e., the state from HRS to LRS can be changed by applying reverse voltage pulses). In the RS operation, the changes from the SET to RESET process indicate an ‘ON’ state and the opposite behavior indicates an ‘OFF’ state [51,52]. The variation of the resistance state in most of the memristors depends on the change of redox potential and is mainly attributed to one of the two phenomena observed: valence change mechanism (VCM) and electrochemical metallization (ECM). The ECM devices are also called conductive bridging cells, wherein electrochemical metal deposition and dissolution are employed purposely to induce RS [53,54].

Such devices are usually constructed from an electrochemically active metal electrode, solid active layer, and an electrochemically inert counter electrode (Figure 2B). In certain traditional metal oxide-based memristors, VCM involves anion migration. This redox reaction results in a valence change of the cation sublattice, which leads to change of the resistance and, consequently, conductivity of the active layer. However, the ECM mechanism depends on the electrochemical nature of either electrode and/or drift of the metal cations. Therefore, the presence of electrochemically active electrodes such as Ag^+ and Cu^{2+} is a prime requirement for ECM-based devices.

MXenes and their basic properties

MXenes have a general formula of $\text{M}_{n+1}\text{X}_n\text{T}_x$ ($n = 1$ to 3), where M is an early transition metal, X is carbon and/or nitrogen, and T_x refers to surface terminations ($-\text{OH}$, $-\text{O}$, $-\text{Cl}$, and/or $-\text{F}$) that are bonded to the peripheral M layers [35]. The general synthetic approach involves selective etching of A layers from MAX precursors using fluoride-containing acidic solutions, during which surface terminations are added [36]. Besides, many top-down and bottom-up strategies, such as using fluoride-based salts, molten salts etchants, alkaline etchants, chemical vapor deposition (CVD), mechanical stripping, and hydrothermal processes, are explored for the synthesis of MXenes [37,55–58]. However, most synthesis methods still rely on fluoride-based etchants because of the high selectivity to etch the A element from the **MAX phase**. Delamination of MXenes into single or few flakes has become a hot research topic as the several layer-dependent properties mainly exist in atomically thin nanosheets, which is achieved by MXene intercalation with polar/large organic molecules between the layers, resulting in a colloidal solution of delaminated MXenes [59]. Moreover, while etching with halide salts and acid (e.g., LiF and HCl), MXenes are intercalated with metal cations further, leading to delamination without any additional steps [59]. To date, about six different possible structures of MXenes have been identified from computational studies [60]. The crystal structure of MXenes is identical to that of the parent MAX phases, where the M atoms are six-coordinated and X atoms occupy the octahedral sites. The overall structure is hexagonally close packed (Figure 2C). Modification of surface terminations and surface functional groups is a critical variable in expanding the properties of MXenes, which is strongly influenced by etching methods [61]. The strong bond between M atoms and $-\text{O}$ terminations make them mechanically much stronger than $\text{M}-\text{OH}$ and $\text{M}-\text{F}$ counterparts [59]. It is also observed that electronic conductivity of Ti- and Mo-based MXenes is enhanced after removal of surface terminations [39] and substituting $-\text{F}$ and $-\text{OH}$ with $-\text{O}$ terminations showed an increase in their band gap [62]. Although several theoretical calculations have made correlation of surface terminations with their electronic properties, very few experimental studies have been reported so far. Furthermore, it has been predicted that $-\text{F}$ terminated Ti_3C_2 demonstrates better thermal conductivity than $-\text{O}$ terminated [63]. Density functional theory calculations show that the presence of Ti atoms on the surface of pristine MXenes contributes to their magnetic property, while surface-terminated MXenes may lose this characteristic [64]. Also, the catalytic activity of MXenes is mainly dependent on the composition of surface functional groups [65]. Thin sheets of MXenes show low resistance and transparency in visible light, making them suitable materials for UV light applications [66]. Because of metallic core channels and abundant free electrons, MXenes have also found applications in sensors and electromagnetic interference shielding [67–69].

Growth of MXene thin films

Owing to their complex chemistry, growth of high-quality semiconducting MXene films is challenging. The following subsections summarize various techniques to develop the MXene thin films by solution processing, mainly on the development of thick coating by solution processes and thin coating by atomistic techniques [40,70–72].

Solution processing

Solution processing (i.e., spin, blade, dip, and spray coating) has been employed, depending on solution viscosity, concentration, and sample size. Spin coating is the most suitable for MXene dispersion to the medium range viscosity (~ 10000 mPa) or medium and lower (1–120 mg/ml) concentration range (Figure 3A) [31]. Blade coating requires higher concentration (~ 20 g/ml) or

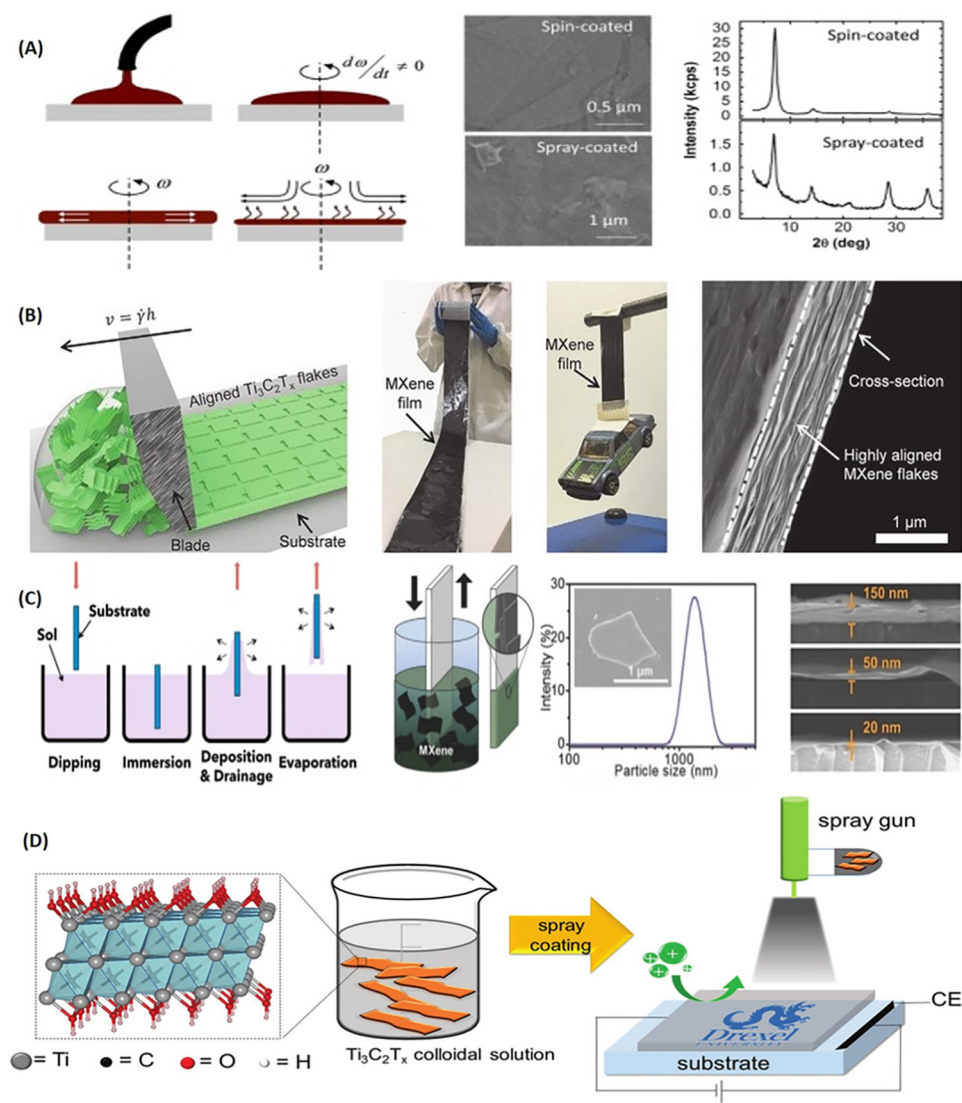


Figure 3. Spin coating of MXene dispersions. (A) Schematic, scanning electron microscopy (SEM) images of spin coated (top) and spray coated (bottom) MXene films with their corresponding X-ray diffraction patterns. Reproduced, with permission, from [106]. (B) Schematic illustration of the blade coating process and digital photograph of a 1-m long and 10-cm wide film produced from large MXene flakes that was blade coated onto a Celgard membrane (thickness of the $\text{Ti}_3\text{C}_2\text{T}_x$ film is 940 nm). Digital photograph of piece of the blade coated $\text{Ti}_3\text{C}_2\text{T}_x$ film (2.0 cm \times 6.5 cm, thickness of 940 nm) made from large flakes lifting ≈ 40 g object. Cross-sectional SEM image of a blade coated film containing highly aligned large MXene flakes [73]. (C) Dip-coating steps to fabricate thin films. Reproduced, with permission, from [98]. Schematic image of optically transparent $\text{Ti}_3\text{C}_2\text{T}_x$ MXene film prepared by dip-coating (left), flake size distribution (right) of MXene dispersion. Cross-sectional SEM images of dip-coated MXene films on glass substrates. Reproduced, with permission, from [107]. (D) Schematic of $\text{Ti}_3\text{C}_2\text{T}_x$ film preparation by spray coating. Shown in the box is the $\text{Ti}_3\text{C}_2\text{T}_x$ structure, whereas Ti, C, O, and H atoms are shown in gray, black, red, and white, respectively. Reproduced, with permission, from [31].

viscosity (up to 2 Pas) of the material, typically best suited for large-scale production (Figure 3B). The better orientation, higher anisotropy, and compacted film morphology with minimum voids results in higher electrical conductivity of the MXene film compared with that of similar thickness films prepared by spin-coating [73]. Dip coating is yet another technique widely accepted for the scale-up fabrication of large-area thin films, suitable for a low viscosity of MXene dispersion (typically resulting in relatively thick films) (Figure 3C). Spray coating is useful when the viscosity of the MXene dispersion is relatively low (concentration <0.36 mg/ml) (Figure 3D) [74]. This allows fast fabrication of the thin film (μm -to-nm range) on a large-area substrate for scale-up. Spray deposition has obvious advantages: easy use, large area coverage, and suitable for any surface. However, spray coating is less uniform and often produces rougher films compared with that of spin coating [31,75,76]. Printing is another solution processing technique that offers large-scale device fabrication at a low cost [77]. A summary of solution processing techniques is tabulated in Table 1 for comparison.

Physical vapor deposition (PVD)

PVD essentially builds the materials atomically from the bottom-up to develop nearly defect-free thin films, with specific orientations and structures that are impossible via solution processing. Sputtering is the most common PVD technique used for the development of MXene films, where individual material sources are used to sputter and control the phase of the film with excellent reproducibility [78]. Cr_2GeC [79] and Cr_2AlC [80] are the most common MXenes that can be deposited by PVD at a lower temperature (500°C). Furthermore, the typical high temperature processing (700–1000°C) is vulnerable to temperature-sensitive substrates, specifically, Ti-based MAX phases.

Table 1. A summary of the performance and working mechanisms of MXene-based memristors

Performance of MXene-based memristor devices						
Memristor material	RS material	Substrate	Operating voltage (V)	Retention (s)	Refs	
Al/Ti ₃ C ₂ @PVP/ITO	Ti ₃ C ₂ @PVP	PEN	−3.0 to 3.0	50 000	[90]	
Al/Ti ₃ C ₂ T _x /Pt/Ti/SiO ₂ /Si	Ti ₃ C ₂ T _x	Pt/Ti/SiO ₂ /Si	−6.0 to 6.0	100 000	[27]	
Cu/Ti ₃ C ₂ /SiO ₂ /W	Ti ₃ C ₂ /SiO ₂	Si wafers	−2.0 to 2.5	1000	[108]	
TiN/Cu/MXene/SiO ₂ /TiN	MXene/SiO ₂	Si wafers	−2.0 to 2.0	20 000	[95]	
Cu/MXene/SiO ₂ /W	MXene/SiO ₂	Si wafers	−2.4 to 2.4	3000	[26]	
Cu/MXene/Cu	MXene	SiO ₂ /Si wafers	−0.8 to 0.8	NA	[89]	
Au/Ti ₃ C ₂ T _x -PVP/rGO	Ti ₃ C ₂ T _x -PVP	SiO ₂ /Si	−2.0 to 2.0	80 000	[109]	
Cu/MXene/SiO ₂ /W	MXene/SiO ₂	Si wafers	−2.4 to 2.4	NA	[110]	
Au/MQDs-PVP/ITO	MQDs-PVP	ITO	−3.0 to 3.0	12 000	[97]	
TiN/Cu/MXene/SiO ₂ /TiN	MXene/SiO ₂		−2.0 to 3.0	3500	[28]	
Al/Ti ₃ C ₂ T _x -OP/ITO	Ti ₃ C ₂ T _x -OP	ITO/glass	−5.0 to 5.0	4000	[25]	
Au/MXene/ pentacene/Au	MXene-TiO ₂	SiO ₂ /Si	NA	10 000	[111]	
MXene solution concentration and film thickness achieved by different coating techniques						
Process	MXene concentration (mg/ml)	Film thickness range	Conductivity	Throughput	Example	Refs
Spin coating	1–120	nm– μm (>20 nm)	Good	Low	Ti ₃ C ₂ T _x	[112]
Blade coating	>20	nm– μm (>200 nm)	Excellent	Medium	Ti ₃ C ₂	[113]
Dip coating	1–10	0.02–0.5 μm	Good	Low	Ti ₃ AlC ₂	[114]
Spray coating	0.1–30	100–250 μm	Very good	Medium	Ti ₃ C ₂	[70]
Inkjet printing	1–36	0.1–0.7 μm	Good	Medium	Ti ₃ C ₂ T _x	[115]
Screen printing	1–5	~ 1–100 μm	Very good	High	Ti ₃ C ₂ T _x	[116]

CVD

Most of the bulk synthesis of MXenes at thermodynamic equilibrium by chemical reactions occurs at high temperature, which is analogous to one of the CVD processes. This is in contrast to PVD, which takes place far from thermodynamic equilibrium under kinetically limited conditions; this provides some control over the growth of lateral size. Nickl and colleagues reported for the first time MXene films (Ti_3SiC_2) by a CVD method in 1972 [81]. Compared with PVD, formation of pure phase Ti_3SiC_2 films via CVD is challenging and also requires a much higher temperature (1000–1300°C). It has been observed that formation of Ti_3SiC_2 includes simultaneous deposition of all three elements and chemical reaction between the gas and solid phase such as TiC, which is therefore also known as reactive CVD [81]. Overall, CVD has been used to a rather limited extent for synthesis of MXene phases and there is room for future research, notably to synthesize MXene phases other than Ti_3SiC_2 by CVD.

MXene-based RS memristors, synapses, and neuromorphic computation

RS devices are considered one of the most competitive candidates as electronic synapses due to their low power consumption, high speed switching, and multiple resistance states [21,22,82–84]. Highly conductive materials such as conductive metal oxides, metals, carbon nanotubes, and graphene are used as electrodes. Among these, conductive metal oxides such as indium-tin oxide (ITO) and fluorine-tin oxide (FTO) can be flexible when used as a thin-film electrode [85]. The flexibility of MXenes provides additional advantages of maintaining the mechanical and electrical properties of the memristor device. Furthermore, the intrinsic properties of MXenes such as ultrahigh conductivity, fast charge response, high stacking density, and hydrophilicity into the structure make them suitable for memristor applications [86,87]. The device structure consists of the MXene as an active layer sandwiched between two electrodes. The device configuration maintains their morphology and robust conductive/switching characteristics while twisted, stretched, or even bent. Considering these advantages, MXenes are a top choice of material for future RS memristor applications [88].

Chen and colleagues have demonstrated that a Cu/MXene/Cu configuration memristor can be used for the development of a high-density brain-inspired neuromorphic computing system without auxiliary circuits [89]. This memristor shows an increase in conductivity with increasing number of voltage pulses with time, suggesting that the conductivity of the memristor is changing with increasing number of pulses with time. This type of spike-dependent conductivity is a key property of biological neurons, which can be mimicked by the memorizer device. The first MXene-based memristor was developed by Han and colleagues in 2019 [90], where a metal-insulator-metal structure comprised of a Ti_3C_2 @polyvinylpyrrolidone (PVP) active layer sandwiched between an Al top electrode and an ITO bottom electrode was constructed on a polyethylene naphthalate (PEN) flexible substrate (Figure 4). The Ti_3C_2 @PVP-based memristor showed bipolar RS behavior with a high ON/OFF ratio of 10^4 and good stability with a retention time of 5×10^4 s. However, the devices fabricated using bare MXene or PVP did not show any RS behavior, suggesting that the presence of surface functional groups in Ti_3C_2 and concentration in Ti_3C_2 @PVP plays a critical role in charge trapping and constructing conductive paths. Increase in the Ti_3C_2 concentration decreases the distance between MXene nanosheets and therefore the formation of conductive paths becomes easier and shows lower SET voltage (V_{SET}). Meanwhile, RESET voltage increases due to the shorter distance between adjacent MXene nanosheets, which hinders the rupture of the conductive paths. Practically, high V_{SET} causes high energy consumption to switch the device from the HRS to LRS, while extremely low V_{SET} would lead to low power consumption to switch the device from HRS to LRS. Yan and colleagues reported the potential of $\text{Ti}_3\text{C}_2\text{T}_x$ as a memristor device for use in artificial bio-synapse applications [27]. An $\text{Al}/\text{Ti}_3\text{C}_2\text{T}_x/\text{Pt}$ device was fabricated by thin-layer deposition of $\text{Ti}_3\text{C}_2\text{T}_x$ on Pt by spin coating and demonstrated the bipolar resistance

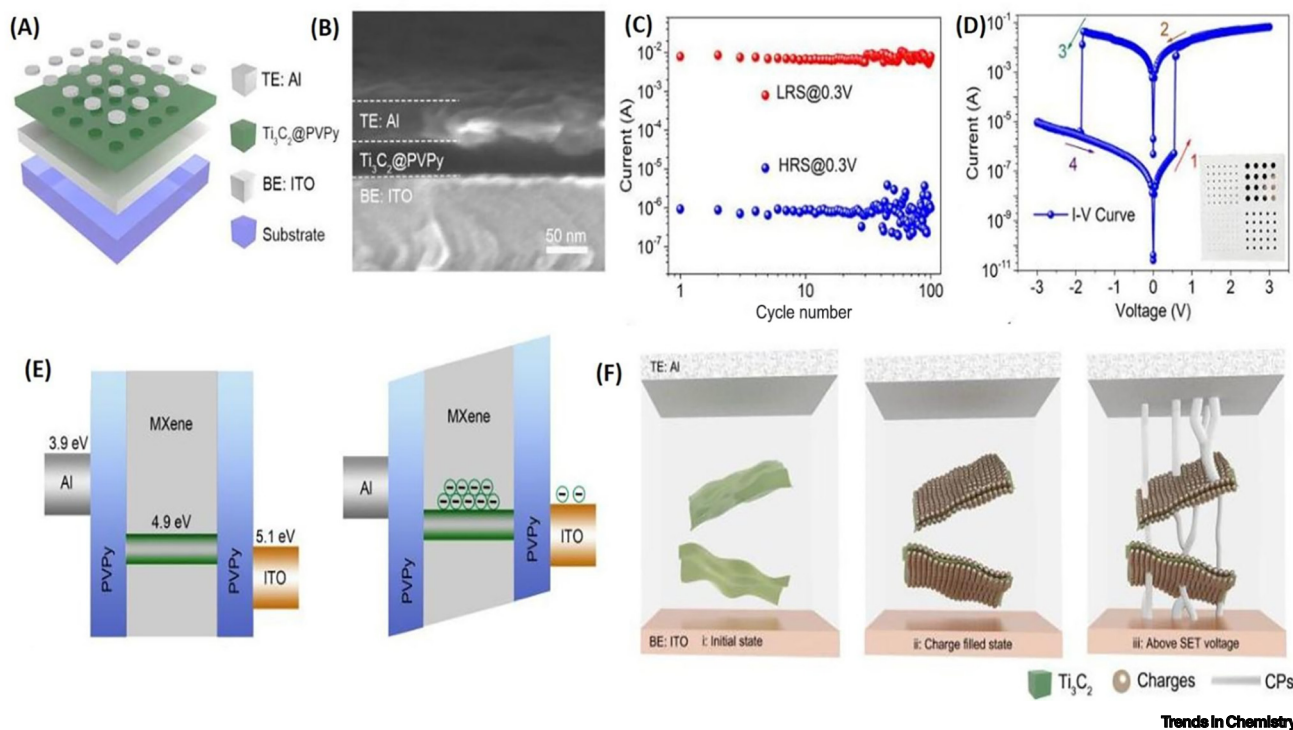
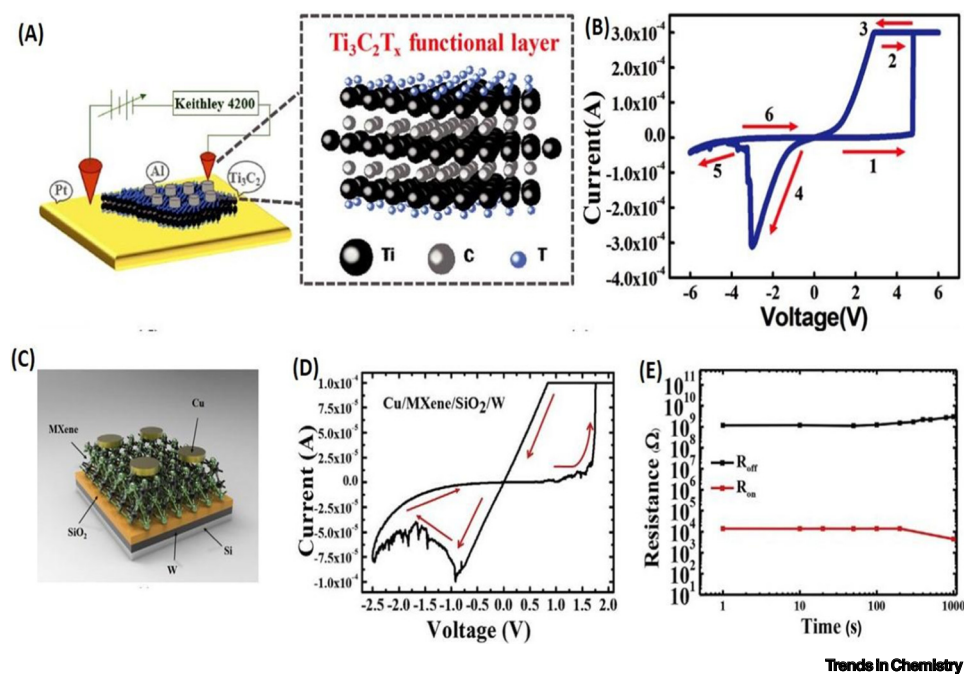


Figure 4. Metal–insulator–metal (MIM) structure, cross-sectional image, electrochemical performance, energy band alignment of resistive random access memory (RRAM) device, and resistive switching (RS) mechanism. (A) MIM structure, (B) cross-sectional scanning electron microscopy image, (C) typical I–V curve, and (D) switching endurance under I–V sweep mode of an MXene (Ti_3C_2)@polyvinylpyrrolidone (PVP)-based RRAM device. (E) Energy band alignment of RRAM device (virgin and under SET process). (F) Illustration of RS mechanism based on charge trapping and conductive paths. Reproduced, with permission, from [90].

switching behavior with a nonvolatile memory effect (Figure 5). The device displayed a retention time of 10^5 s and the resistance of the device could be modulated by minimum pulsed voltage duration as short as 10 ns. Furthermore, the progressive enhancement and inhibition of conductance under different voltage pulses suggests that the memristor device successfully simulates the learning and memory functions of biological synapses. Wei and colleagues demonstrated a graphdiyne-based artificial synapse (GAS), exhibiting intrinsic STP to mimic biological signal transmission behavior. The impulse response of the GAS is reduced to several millivolts with competitive femtowatt-level consumption, exceeding the biological level by orders of magnitude, which makes them potential candidates for soft electronics, neurobotics, and biohybrid systems of brain–computer interfaces [91].

Tong and colleagues fabricated a $Cu/Ti_3C_2/SiO_2/W$ memristor device, where Cu and W were the active top and inert bottom electrodes, respectively, and Ti_3C_2/SiO_2 as the RS layer film was obtained by spin coating. MXene memristors showed resistance transforms between HRS and LRS under voltage stimulus with retention of 1000 s in both on and off states. The results shown by the MXene-containing memristor device were better than those of the MXene-free device ($Cu/SiO_2/W$), suggesting that the MXene helps to lower the operating voltage and enhance the device stability [92,93]. This can be attributed to the observation that high mobility of Cu in SiO_2 could be beneficial for lower energy operation but has a negative effect on the stability of the memristor [94]. Furthermore, the presence of MXene reduces the mobility of Cu ions in the resistance switching layer of the memristor, which leads to growth of the CF from the top electrode instead

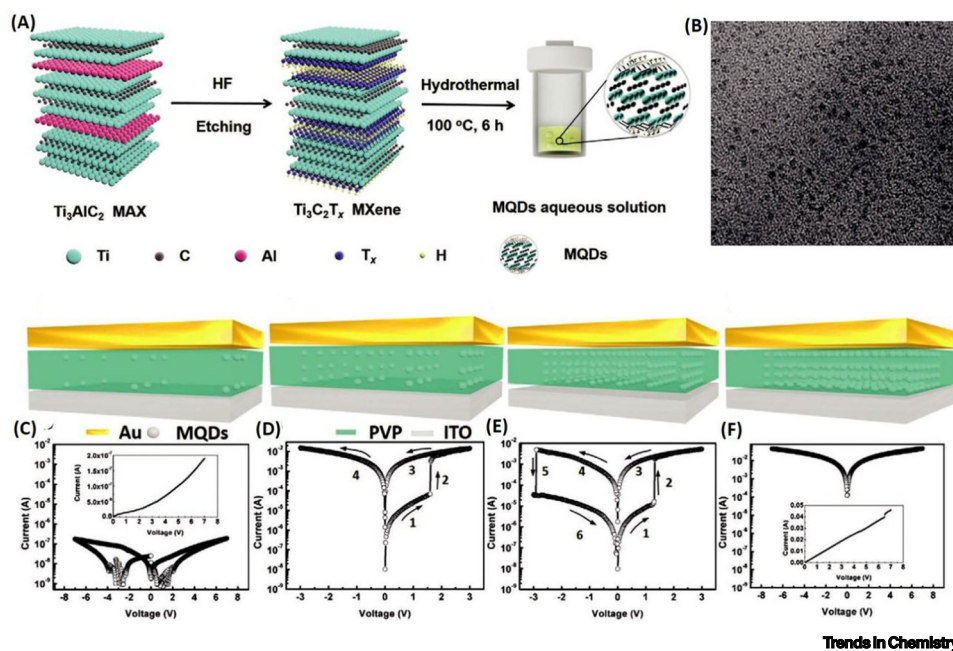


Trends in Chemistry

Figure 5. Schematic of the $\text{Al}/\text{Ti}_3\text{C}_2\text{T}_x/\text{Pt}$ device and electrochemical behavior of the $\text{Cu}/\text{Ti}_3\text{C}_2/\text{SiO}_2/\text{W}$ memristor device. (A) Schematic structure of the $\text{Al}/\text{Ti}_3\text{C}_2\text{T}_x/\text{Pt}$ device and (B) typical I-V curves of the device (the red arrow indicates direction of voltage sweep). Reproduced, with permission, from [27]. (C) Schematic illustration, (D) I-V characteristics, and (E) retention of different resistance states in the $\text{Cu}/\text{Ti}_3\text{C}_2/\text{SiO}_2/\text{W}$ memristor device. Reproduced, with permission, from [108].

of the bottom electrode produced by redox (and fewer in number due to the decrease of Cu mobility). Tong and coworkers further studied the performance of RS devices in the form of cross-bar arrays with and without MXene material [95]. The two device structures $\text{TiN}/\text{Cu}/\text{SiO}_2/\text{TiN}$ and $\text{TiN}/\text{Cu}/\text{MXene}/\text{SiO}_2/\text{TiN}$ were fabricated on Si wafer using a silicon compatible process to study the effect of the MXene. The introduction of MXene changes the electric field distribution at the interface between the metal electrode and oxide and, as a result, a conductive path is easily formed, which in turn lowers the operating voltage and attains low power consumption. Furthermore, the presence of MXene brings more stable resistance states in the device due to the uniform and systematic growth of CFs along with the direction of MXene nanostructures, which improves the performance of RS devices [95].

MXene-derived quantum dots (MQDs) have also attracted great research interest due to their size and quantum confinement effects. Compared with MXene nanosheets, MQDs could be a safe and reliable RS material for upcoming nonvolatile data storage due to their strong quantum confinement, edge effects, and hydrophilicity [96]. Furthermore, MQDs disperse well in water-soluble polymers for charge trapping and subsequently improve the reliability of data storage. Mao and colleagues first reported the synthesis of MQDs by a hydrothermal synthetic method using $\text{Ti}_3\text{C}_2\text{T}_x$ etched by hydrofluoric acid [97]. The nonvolatile storage behavior of the resulting ITO/MQDs-PVPy/Au storage device was fine-tuned by carefully controlling the doping content of MQDs in PVP (Figure 6). Sun and colleagues effectively utilized octylphosphonic acid for surface modification of $\text{Ti}_3\text{C}_2\text{T}_x$ through hydrogen bonding so that phosphorus could uniformly distribute on the monolayer $\text{Ti}_3\text{C}_2\text{T}_x$ nanosheets [25]. MXene surface treated with phosphonic acid ensures and promotes the stability of modified MXene in organic solutions [98]. Additionally,

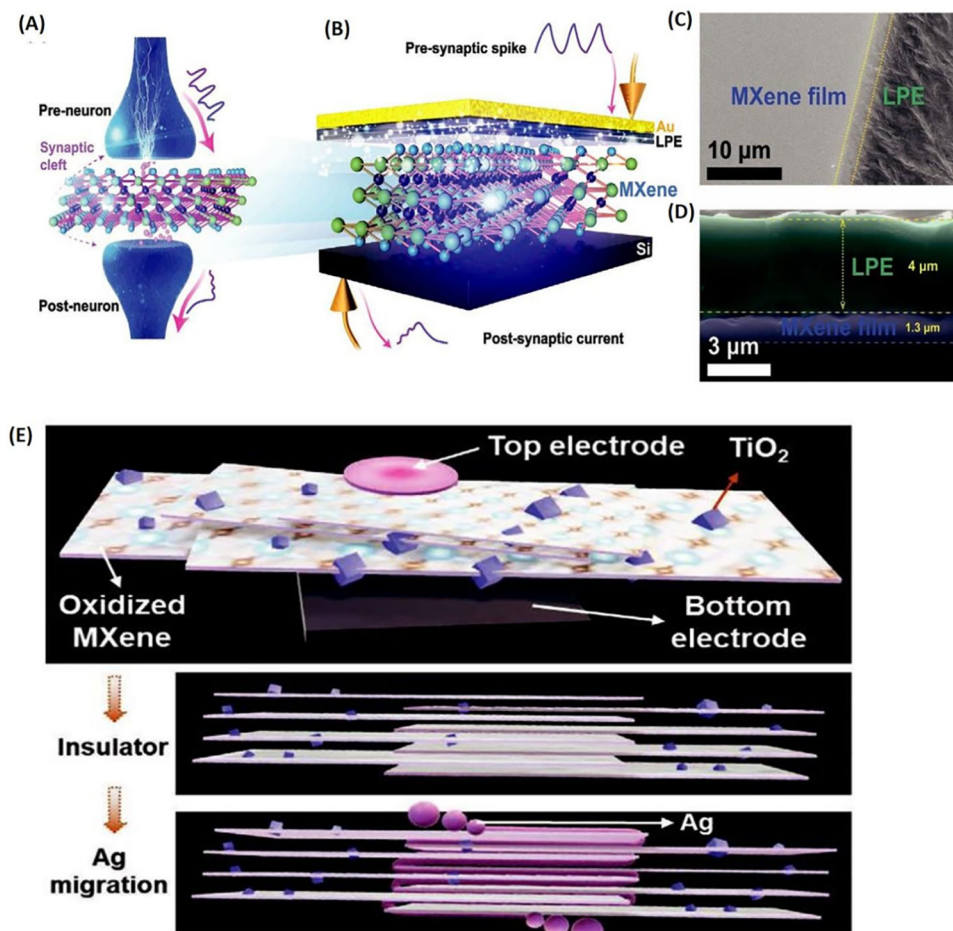


Trends in Chemistry

Figure 6. Schematic and transmission electron microscopy (TEM) image for the synthesis and characterization of MXene-derived quantum dots (MQDs), along with I-V curve characteristics of the device. (A) Schematic illustration of the synthesis and (B) TEM image of MQDs. Increase of MQD content in MQDs-polyvinylpyrrolidone (PVP) memory device as (C) ≈ 20 $\mu\text{g/ml}$, (D) ≈ 380 $\mu\text{g/ml}$, (E) ≈ 1.14 mg/ml , and (F) ≈ 3.42 mg/ml and corresponding I-V characteristic curves of the device under different MQD contents. Abbreviations: HF, hydrofluoric acid; ITO, indium-tin oxide. Reproduced, with permission, from [97].

octylphosphorus acid can self-assemble on multilayered MXene surfaces. A flexible storage device on polyethylene terephthalate (PET) substrate ($\text{Al/Ti}_3\text{C}_2\text{T}_x\text{-OP MXene/PET}$) was fabricated, which maintained good distinguishable multilevel storage characteristics even after 5000 bending cycles at a radius of curvature ρ of 2.1 cm.

Wei and colleagues coupled the Ti_3C_2 nanosheets with a solid lithium-polymer-electrolyte layer to mimic the synaptic functions (Figure 7), including paired-pulse facilitation, SRDP, dendritic integration, and memory enhancement [99]. The integral large interlayer spacing and good conductivity of MXene benefit the storage and easy release of ions. Later, Wang and colleagues explored the idea of Ag nanoparticle doping to improve the electronic performance of the Ti_3C_2 -based memristor [100]. However, the device based on Ag has limitations because the Ag electrodes of traditional memristors would dissolve gradually due to the electrochemical reaction, leading to the deterioration of electrical properties of MXene-based devices. Therefore, this study suggested replacing active Ag electrodes with inert Al electrodes and doping Ag nanoparticles into the MXene-based functional layer of the memristor. Furthermore, doping of Ag not only enhances the electronic performance and neuro-bionic properties of the MXene memristor but also resolves the issue related to the current abrupt behavior of MXene devices, which realizes the bidirectional continuous current transition in switching processes. Additionally, the energy consumption of the $\text{Al/Ti}_3\text{C}_2\text{:Ag/Pt}$ device is around ten-fold lower than that of the pure Ti_3C_2 device. In general, MXene sheets have high surface functional groups, which can easily facilitate low power diffusive memory devices. However, high electrical conductivity of these sheets hampers their applications in threshold switching. MXenes are not very stable at high temperatures and are prone to partial oxidation. Few TiO_2 particles are formed in these partially oxidized



Trends in Chemistry

Figure 7. Schematics for biological synapses and Ti_3C_2 -MXene artificial synapses, and images of an MXene/lithium-polymer-electrolyte (LPE) film. Schematic illustration of (A) biological synapse and (B) Ti_3C_2 -MXene artificial synapses. (C) Scanning electron microscopy image and (D) cross-section image of MXene/LPE film. Reproduced, with permission, from [99]. (E) Schematic illustration of partially oxidized MXene-based device. Reproduced, with permission, from [101].

MXene sheets, which not only decreases the conductivity but also serves as spacers between MXene sheets, hindering the contacts and restacking (Figure 7E) [101]. As a result, MXene sheets can be used for Ag diffusive memory devices as TiO_2 acts as a spacer and provides a path for Ag^+ migration [36]. Migration of silver ions via MXene sheets is a key of modulated conductance of the device based on threshold switching characteristics. As a result, the device exhibits threshold RS characteristics based on silver ion migration dynamics. The mechanism of RS memory devices is greatly influenced by the switching materials, electrodes, device structures, and environmental conditions [102]. To achieve the desired memory properties from RS devices is to judiciously engineer the top electrode [103].

Concluding remarks

In the era of AI and Internet of Things, memory cells are attracting great attention and importance, especially in low-power, flexible, and portable information storage systems as well as neuromorphic computing. MXenes have great potential as the material of choice due to storage density and

Outstanding questions

Can surface engineering the MXene-based memristor, such as surface termination of the same kind or proportional distribution of different surface terminations, improve the performance?

How can the design of MXene-based heterostructures with transition metal oxides, perovskites, and polymers be optimized in order to increase the performance? And what are the key roles of these integrated functional materials?

How can we accurately adjust the synapse weight of the MXenes to increase the number of pulses before it reaches saturation and prior to the completion of STP and LTP?

capacity that can reach the level of traditional inorganic metal oxide memristor in the future. The recent advances in the computationally intensive and resource hungry ML and deep learning architectures require efficient and scalable computing systems. Here, progress in MXene-based memristors is summarized and discussed with synthesis, thin film growth, current switching mechanism, and applications. Various solution-processible methods have been successfully employed to fabricate thin films and devices, which can be tested to investigate the effects of charge injection and modulate the interface barrier. Additionally, the simple structure and excellent compatibility of two-terminal electronic devices enable it to perform concurrent learning and parallel data processing, opening the possibility of developing a robust neural network with significantly fewer neurons. Development of highly integrated 3D synaptic electronics with multiple input and output signal transitions are expected to be mimicked to realize the full synaptic functions of the artificial nerve network. Detailed and controllable studies are necessary to determine the impact of MXene composition, particularly non-Ti₃C₂, and surface modification on MXene-based devices, especially since surface terminations may affect the resulting performance (see [Outstanding questions](#)). Furthermore, development of nonmetallic MXenes and their experimental realization could be challenging at this stage of MXene-based memristor development. Finally, when it comes to MXenes for AI, we believe that the field is still in its infancy and many important developments are yet to come. Some of these prospective developments, such as the realization of artificial general intelligence and artificial super intelligence demand heavy computation of several petaflops, which is almost impossible using traditional computer architecture such as von Neumann architecture. In this regard, the efficient and analog computing alternatives such as neuromorphic computing may play a significant role. We believe 2D materials such as MXenes could be a major player for this development.

Acknowledgments

This study was financially supported by the Department of Science and Technology (DST), India under the joint India-Korea project (INT/Korea/P-52). A.S. and M.R. gratefully acknowledge the financial support from Science and Engineering Research Board (SERB) core research grant CRG/2020/000869 and GUJCOST/STI/2021-22/3873 from the Government of Gujarat, India to perform this study. N.C., A.S., and M.R. would also like to thank Pandit Deendayal Energy University (PDEU) for the financial support under start-up grant ORSP/R&D/PDPU/2021/NC00/R0069, ORSP/R&D/PDPU/2019/AS00/ROO47, and ORSP/R&D/PDPU/2019/MR/RO051.

Declaration of interests

No interests are declared.

References

1. Lecun, Y. *et al.* (2015) Deep learning. *Nature* 521, 436–444
2. Khot, A.C. *et al.* (2021) Ti₃C₂-based MXene oxide nanosheets for resistive memory and synaptic learning applications. *ACS Appl. Mater. Interfaces* 13, 5216–5227
3. Schmidt, J. *et al.* (2019) Recent advances and applications of machine learning in solid-state materials science. *NPJ Comput. Mater.* 5, 83
4. Maass, W. *et al.* (2019) Brain computation: a computer science perspective. In *Computing Software and Science. Lecture Notes in Computer Science* (Vol. 10 000) (Steffen, B. and Woeginger, G., eds), pp. 184–199, Springer
5. Marois, R. and Ivanoff, J. (2005) Capacity limits of information processing in the brain. *Trends Cogn. Sci.* 9, 296–305
6. Von Neumann, J. (1958) *The Computer and The Brain*, Yale University Press
7. Wang, T.Y. *et al.* (2020) Ultralow power wearable heterosynapse with photoelectric synergistic modulation. *Adv. Sci.* 7, 1903480
8. Drubach, D. (2000) *The Brain Explained*, Prentice-Hall
9. Rigden, J.S. (1996) *Macmillan Encyclopedia of Physics*, Simon & Schuster Macmillan
10. Peláez, E. (1990) Parallelism and the crisis of von Neumann computing. *Technol. Soc.* 12, 65–77
11. Mead, C. (1990) Neuromorphic electronic systems. *Proc. IEEE* 78, 1629–1636
12. Pereda, A.E. (2014) Electrical synapses and their functional interactions with chemical synapses. *Nat. Rev. Neurosci.* 15, 250–263
13. Saighi, S. *et al.* (2015) Plasticity in memristive devices for spiking neural networks. *Front. Neurosci.* 9, 51
14. Pan, Y. *et al.* (2018) Mimicking synaptic plasticity and learning behaviours in solution processed SnO₂ memristor. *J. Alloys Compd.* 757, 496–503
15. Mehonic, A. *et al.* (2020) Memristors—from in-memory computing, deep learning acceleration, and spiking neural networks to the future of neuromorphic and bio-inspired computing. *Adv. Intell. Syst.* 2, 2000085
16. Wang, Y. *et al.* (2021) An in-memory computing architecture based on two-dimensional semiconductors for multiply-accumulate operations. *Nat. Commun.* 12, 3347
17. Yu, J. *et al.* (2018) Memristive devices for computation-in-memory. In *Proceedings of 2018 Design, Automation & Test in Europe Conference & Exhibition*, pp. 1646–1651, IEEE, Dresden, Germany
18. Ilarionov, G.A. *et al.* (2020) Memristive TiO₂: synthesis, technologies, and applications. *Front. Chem.* 8, 724

19. Pan, X. *et al.* (2016) Rectifying filamentary resistive switching in ion-exfoliated LiNbO₃ thin films. *Appl. Phys. Lett.* 108, 032904
20. Hu, P. *et al.* (2018) Synaptic behavior in metal oxide-based memristors. In *Advances in Memristor Neural Networks* (Ciufudean, C., ed.), pp. 3–22, IntechOpen
21. Gogoi, H.J. *et al.* (2021) Advances in flexible memristors with hybrid perovskites. *J. Phys. Chem. Lett.* 12, 8798–8825
22. Solanki, A. *et al.* (2019) Interfacial mechanism for efficient resistive switching in Ruddlesden–Popper perovskites for non-volatile memories. *J. Phys. Chem. Lett.* 11, 463–470
23. Kumbhar, D. *et al.* (2022) Forming free non-volatile resistive switching mechanism in Ruddlesden Popper perovskite memristors. In *2022 International Conference for Advancement in Technology, Barcelona, Spain*
24. Li, Y. *et al.* (2017) Resistive switching performance improvement via modulating nanoscale conductive filament, involving the application of two-dimensional layered materials. *Small* 13, 1604306
25. Sun, W.-J. *et al.* (2020) Surface functionalization of single-layered Ti₃C₂T_x MXene and its application in multilevel resistive memory. *ACS Appl. Mater. Interfaces* 12, 9865–9871
26. Lian, X. *et al.* (2019) Resistance switching characteristics and mechanisms of MXene/SiO₂ structure-based memristor. *Appl. Phys. Lett.* 115, 063501
27. Yan, X. *et al.* (2019) A new memristor with 2D Ti₃C₂T_x MXene flakes as an artificial bio-synapse. *Small* 15, 1900107
28. He, N. *et al.* (2020) Demonstration of 2D MXene memristor: stability, conduction mechanism, and synaptic plasticity. *Mater. Lett.* 266, 127413
29. Naguib, M. *et al.* (2011) Two-dimensional nanocrystals produced by exfoliation of Ti₃AlC₂. *Adv. Mater.* 23, 4248–4253
30. Pang, J. *et al.* (2019) Applications of 2D MXenes in energy conversion and storage systems. *Chem. Soc. Rev.* 48, 72–133
31. Hantanasirisakul, K. *et al.* (2016) Fabrication of Ti₃C₂T_x MXene transparent thin films with tunable optoelectronic properties. *Adv. Electron. Mater.* 2, 1600050
32. Ibragimova, R. *et al.* (2021) Surface functionalization of 2D MXenes: trends in distribution, composition, and electronic properties. *J. Phys. Chem. Lett.* 12, 2377–2384
33. Ma, F. *et al.* (2020) Optoelectronic perovskite synapses for neuromorphic computing. *Adv. Funct. Mater.* 30, 1908901
34. Wang, M. *et al.* (2018) Robust memristors based on layered two-dimensional materials. *Nat. Electron.* 1, 130–136
35. Gogotsi, Y. and Anasori, B. (2019) The rise of MXenes. *ACS Nano* 13, 8491–8494
36. Alhabeib, M. *et al.* (2017) Guidelines for synthesis and processing of two-dimensional titanium carbide (Ti₃C₂T_x MXene). *Chem. Mater.* 29, 7633–7644
37. Liu, F. *et al.* (2017) Preparation of Ti₃C₂ and Ti₂C MXenes by fluoride salts etching and methane adsorptive properties. *Appl. Surf. Sci.* 416, 781–789
38. Lipatov, A. *et al.* (2018) Elastic properties of 2D Ti₃C₂T_x MXene monolayers and bilayers. *Sci. Adv.* 4, eaat0491
39. Hart, J.L. *et al.* (2019) Control of MXenes' electronic properties through termination and intercalation. *Nat. Commun.* 10, 522
40. Schultz, T. *et al.* (2019) Surface termination dependent work function and electronic properties of Ti₃C₂T_x MXene. *Chem. Mater.* 31, 6590–6597
41. Rajan, A.C. *et al.* (2018) Machine-learning-assisted accurate band gap predictions of functionalized mxene. *Chem. Mater.* 30, 4031–4038
42. Kim, H. *et al.* (2019) MXetronics: electronic and photonic applications of MXenes. *Nano Energy* 60, 179–197
43. Karbalaee Akbari, M. and Zhuiykov, S. (2019) A bioinspired optoelectronically engineered artificial neurobotics device with sensorimotor functionalities. *Nat. Commun.* 10, 3873
44. Gao, S. *et al.* (2019) Organic and hybrid resistive switching materials and devices. *Chem. Soc. Rev.* 48, 1531–1565
45. Wang, Y. *et al.* (2018) Photonic synapses based on inorganic perovskite quantum dots for neuromorphic computing. *Adv. Mater.* 30, 1802883
46. Khalid, M. (2019) Review on various memristor models, characteristics, potential applications, and future works. *Trans. Electr. Electron. Mater.* 20, 289–298
47. Strukov, D.B. *et al.* (2008) The missing memristor found. *Nature* 453, 80–83
48. Oğuz, Y. (2018) Mathematical modeling of memristors. In *Memristor and Memristive Neural Networks*, IntechOpen
49. Dearnaley, G. *et al.* (1970) Electrical phenomena in amorphous oxide films. *Rep. Prog. Phys.* 33, 1129
50. Waser, R. and Aono, M. (2007) Nanoionics-based resistive switching memories. *Nat. Mater.* 6, 833–840
51. Ielmini, D. (2016) Resistive switching memories based on metal oxides: mechanisms, reliability and scaling. *Semicond. Sci. Technol.* 31, 063002
52. Zahoor, F. *et al.* (2020) Resistive random access memory (RRAM): an overview of materials, switching mechanism, performance, multilevel cell (mlc) storage, modeling, and applications. *Nanoscale Res. Lett.* 15, 90
53. Kozicki, M.N. *et al.* (2005) Nanoscale memory elements based on solid-state electrolytes. *IEEE Trans. Nanotechnol.* 4, 331–338
54. Liu, G. *et al.* (2018) Recent advances in resistive switching materials and devices: from memories to memristors. *Eng. Sci.* 4, 4–43
55. Li, M. *et al.* (2019) Element replacement approach by reaction with Lewis acidic molten salts to synthesize nanolaminated MAX phases and MXenes. *J. Am. Chem. Soc.* 141, 4730–4737
56. Li, T. *et al.* (2018) Fluorine-free synthesis of high-purity Ti₃C₂T_x (T=OH, O) via alkali treatment. *Angew. Chem.* 57, 6115–6119
57. Xu, C. *et al.* (2015) Large-area high-quality 2D ultrathin Mo₂C superconducting crystals. *Nat. Mater.* 14, 1135–1141
58. Anasori, B. *et al.* (2017) 2D metal carbides and nitrides (MXenes) for energy storage. *Nat. Rev. Mater.* 2, 16098
59. Hemanth, N.R. *et al.* (2021) Transition metal dichalcogenide-decorated MXenes: promising hybrid electrodes for energy storage and conversion applications. *Mater. Chem. Front.* 5, 3298–3321
60. Ronchi, R.M. *et al.* (2019) Synthesis, structure, properties and applications of MXenes: current status and perspectives. *Ceram. Int.* 45, 18167–18188
61. Hope, M.A. *et al.* (2016) NMR reveals the surface functionalisation of Ti₃C₂ MXene. *Phys. Chem. Chem. Phys.* 18, 5099–5102
62. Liu, P. *et al.* (2020) Surface termination modification on high-conductivity MXene film for energy conversion. *J. Alloys Compd.* 829, 154634
63. Gholivand, H. *et al.* (2019) Effect of surface termination on the lattice thermal conductivity of monolayer Ti₃C₂T_x MXenes. *J. Appl. Phys.* 126, 065101
64. Xie, Y. and Kent, P.R.C. (2013) Hybrid density functional study of structural and electronic properties of functionalized Tin+1Xn (X=C, N) monolayers. *Phys. Rev. B - Condens. Matter Mater. Phys.* 87, 235441
65. Niu, K. *et al.* (2021) Structure-activity correlation of Ti₂CT₂ MXenes for C–H activation. *J. Phys. Condens. Matter* 33, 235201
66. VahidMohammadi, A. *et al.* (2021) The world of two-dimensional carbides and nitrides (MXenes). *Science* 372, eabf1581
67. Shahzad, F. *et al.* (2016) Electromagnetic interference shielding with 2D transition metal carbides (MXenes). *Science* 353, 1137–1140
68. Liu, J. *et al.* (2017) Hydrophobic, flexible, and lightweight MXene foams for high-performance electromagnetic-interference shielding. *Adv. Mater.* 29, 1702367
69. Pei, Y. *et al.* (2021) Ti₃C₂TXMXene for sensing applications: recent progress, design principles, and future perspectives. *ACS Nano* 15, 3996–4017
70. Wang, Z. *et al.* (2018) Oxide thin-film electronics using all-MXene electrical contacts. *Adv. Mater.* 30, 1706656
71. Chaudhuri, K. *et al.* (2018) Highly broadband absorber using plasmonic titanium carbide (MXene). *ACS Photonics* 5, 1115–1122
72. Kang, Z. *et al.* (2017) MXene–silicon van der Waals heterostructures for high-speed self-driven photodetectors. *Adv. Electron. Mater.* 3, 1700165
73. Zhang, J. *et al.* (2020) Scalable manufacturing of free-standing, strong Ti₃C₂T_x MXene films with outstanding conductivity. *Adv. Mater.* 32, 2001093
74. Abdolhosseinzadeh, S. *et al.* (2020) Printing and coating MXenes for electrochemical energy storage devices. *J. Phys. Energy* 2, 031004
75. Peng, Y.-Y. *et al.* (2016) All-MXene (2D titanium carbide) solid-state microsupercapacitors for on-chip energy storage. *Energy Environ. Sci.* 9, 2847–2854

76. Dillon, A.D. *et al.* (2016) Highly conductive optical quality solution-processed films of 2D titanium carbide. *Adv. Funct. Mater.* 26, 4162–4168
77. Sreenilayam, S.P. *et al.* (2020) Advanced materials of printed wearables for physiological parameter monitoring. *Mater. Today* 32, 147–177
78. Frodelius, J. *et al.* (2010) Sputter deposition from a Ti2AlC target: process characterization and conditions for growth of Ti2AlC. *Thin Solid Films* 518, 1621–1626
79. Eklund, P. *et al.* (2011) Epitaxial growth and electrical transport properties of Cr2GeC thin films. *Phys. Rev. B - Condens. Matter Mater. Phys.* 84, 075424
80. Walter, C. *et al.* (2006) Towards large area deposition of Cr2AlC on steel. *Thin Solid Films* 515, 389–393
81. Mingxing, A. *et al.* (2006) Synthesis of Ti3AlC2 powders using Sn as an additive. *J. Am. Ceram. Soc.* 89, 1114–1117
82. Wang, Z. *et al.* (2016) Memristors with diffusive dynamics as synaptic emulators for neuromorphic computing. *Nat. Mater.* 16, 101–108
83. Yan, X. *et al.* (2019) Vacancy-induced synaptic behavior in 2D WS2 nanosheet-based memristor for low-power neuromorphic computing. *Small* 15, 1901423
84. Prezioso, M. *et al.* (2015) Training and operation of an integrated neuromorphic network based on metal-oxide memristors. *Nature* 521, 61–64
85. Kim, J.-H. *et al.* (2018) Flexible ITO films with atomically flat surfaces for high performance flexible perovskite solar cells. *Nanoscale* 10, 20587–20598
86. Soundiraraju, B. and George, B.K. (2017) Two-dimensional titanium nitride (Ti2N) MXene: synthesis, characterization, and potential application as surface-enhanced Raman scattering substrate. *ACS Nano* 11, 8892–8900
87. Lukatskaya, M.R. *et al.* (2017) Ultra-high-rate pseudocapacitive energy storage in two-dimensional transition metal carbides. *Nat. Energy* 2, 17105
88. Xu, S. *et al.* (2017) Flexible MXene-graphene electrodes with high volumetric capacitance for integrated co-cathode energy conversion/storage devices. *J. Mater. Chem. A* 5, 17442–17451
89. Chen, Y. *et al.* (2019) Realization of artificial neuron using MXene bi-directional threshold switching memristors. *IEEE Electron Device Lett.* 40, 1686–1689
90. Ding, G. *et al.* (2019) Configurable multi-state non-volatile memory behaviors in Ti3C2 nanosheets. *Nanoscale* 11, 7102–7110
91. Wei, H. *et al.* (2021) Mimicking efferent nerves using a graphdiyne-based artificial synapse with multiple ion diffusion dynamics. *Nat. Commun.* 12, 1068
92. Nandakumar, S.R. *et al.* (2016) A 250 mV Cu/SiO2/W memristor with half-integer quantum conductance states. *Nano Lett.* 16, 1602–1608
93. Chen, W. *et al.* (2016) A CMOS-compatible electronic synapse device based on Cu/SiO2/W programmable metallization cells. *Nanotechnology* 27, 255202
94. Belmonte, A. *et al.* (2015) Operating-current dependence of the Cu-mobility requirements in oxide-based conductive-bridge RAM. *IEEE Electron Device Lett.* 36, 775–777
95. He, N. *et al.* (2019) Influence of a novel 2d material MXene on the behavior of memristor and its crossbar array. In *Proceeding of the 2019 IEEE International Conference on Electron Devices and Solid-State Circuits, Xi'an Shi, China*
96. Xue, Q. *et al.* (2017) Photoluminescent Ti3C2 MXene quantum dots for multicolor cellular imaging. *Adv. Mater.* 29, 1604847
97. Mao, H. *et al.* (2020) MXene quantum dot/polymer hybrid structures with tunable electrical conductance and resistive switching for nonvolatile memory devices. *Adv. Electron. Mater.* 6, 1900493
98. Hu, M. *et al.* (2018) Surface functional groups and interlayer water determine the electrochemical capacitance of Ti3C2Tx MXene. *ACS Nano* 12, 3578–3586
99. Wei, H. *et al.* (2021) Redox MXene artificial synapse with bidirectional plasticity and hypersensitive responsibility. *Adv. Funct. Mater.* 31, 2007232
100. Wang, K. *et al.* (2021) MXene Ti3C2 memristor for neuromorphic behavior and decimal arithmetic operation applications. *Nano Energy* 79, 105453
101. Sokolov, A. *et al.* (2021) Partially oxidized MXene Ti3C2Tx sheets for memristor having synapse and threshold resistive switching characteristics. *Adv. Electron. Mater.* 7, 2000866
102. Lee, J.S. *et al.* (2015) Resistive switching phenomena: a review of statistical physics approaches. *Appl. Phys. Rev.* 2, 031303
103. Tran, K.M. *et al.* (2019) Influence of top electrode on resistive switching effect of chitosan thin films. *J. Mater. Res.* 34, 3899–3906
104. Kim, H. *et al.* (2019) Halide perovskites for resistive random-access memories. *J. Mater. Chem. C* 7, 5226–5234
105. Khazaei, M. *et al.* (2017) Electronic properties and applications of MXenes: a theoretical review. *J. Mater. Chem. C* 5, 2488–2503
106. Abdolhosseinzadeh, S. *et al.* (2021) Perspectives on solution processing of two-dimensional MXenes. *Mater. Today* 48, 214–240
107. Salles, P. *et al.* (2018) Automated scalpel patterning of solution processed thin films for fabrication of transparent MXene microsupercapacitors. *Small* 14, 1802864
108. Zhang, M. *et al.* (2019) Formation of new MXene film using spinning coating method with DMSO solution and its application in advanced memristive device. *Ceram. Int.* 45, 19467–19472
109. Gu, C. *et al.* (2019) Facile synthesis of Ti3C2Tx-poly(vinylpyrrolidone) nanocomposites for nonvolatile memory devices with low switching voltage. *ACS Appl. Mater. Interfaces* 11, 38061–38067
110. Wang, Y. *et al.* (2019) Manipulation of the electrical behaviors of Cu/MXene/SiO2/W memristor. *Appl. Phys. Express* 12, 106504
111. Lyu, B. *et al.* (2020) 2D MXene-TiO2 core-shell nanosheets as a data-storage medium in memory devices. *Adv. Mater.* 32, 1907633
112. Mariano, M. *et al.* (2016) Solution-processed titanium carbide MXene films examined as highly transparent conductors. *Nanoscale* 8, 16371–16378
113. Kurra, N. *et al.* (2016) MXene-on-paper coplanar microsupercapacitors. *Adv. Energy Mater.* 6, 1601372
114. Akshay Kumar, K.P. *et al.* (2021) Dip-coating of MXene and transition metal dichalcogenides on 3D-printed nanocarbon electrodes for the hydrogen evolution reaction. *Electrochem. Commun.* 122, 106890
115. Zhang, C. *et al.* (2019) Additive-free MXene inks and direct printing of micro-supercapacitors. *Nat. Commun.* 10, 1795
116. Sreenilayam, S.P. *et al.* (2021) MXene materials based printed flexible devices for healthcare, biomedical and energy storage applications. *Mater. Today* 43, 99–131